Left atrial single-cell transcriptomics reveals amphiregulin as a surrogate marker for atrial fibrillation

Check for updates

Yuya Suzuki [1], Takuo Emoto [1] ✉, Shunsuke Sato[2], Takeshi Yoshida[3], Mitsuhiko Shoda[1],
Hiromi Endoh[4], Manabu Nagao [5], Tomoyo Hamana[1], Taishi Inoue[6], Tomohiro Hayashi [1], Eriko Nitta[4],
Hiroki Konishi[7], Kunihiko Kiuchi [1], Mitsuru Takami[1], Kimitake Imamura[1,8], Masayuki Taniguchi[9],
Masatoshi Inoue[3], Toshihiro Nakamura[1], Yusuke Sonoda[1], Hiroyuki Takahara[1], Kazutaka Nakasone[1],
Kyoko Yamamoto[1], Kenichi Tani[1], Hidehiro Iwai[1], Yusuke Nakanishi[1], Shogo Yonehara[1],
Atsushi Murakami[1], Ryuji Toh[5], Takenao Ohkawa[3], Tomoyuki Furuyashiki [9], Ryo Nitta [4],
Tomoya Yamashita [1,10], Ken-ichi Hirata[1] & Koji Fukuzawa[1,8]

Atrial fibrillation (AF) is strongly associated with strokes, heart failure, and increased mortality. This study aims to identify the monocyte–macrophage heterogeneity and interactions of these cells with non-immune cells, and to identify functional biomarkers in patients with AF. Therefore, we assess the single cell landscape of left atria (LA), using a combination of single cell and nucleus RNA-seq. Myeloid cells in LA tissue are categorized into five macrophage clusters, three monocyte clusters, and others. Cell-Chat analysis revealed that monocytes and IL1B$^+$ macrophages send epidermal growth factor (EGF) signals to fibroblasts. Amphiregulin (AREG) is the most upregulated gene in monocytes and IL1B$^+$ macrophages in the AF group, compared with healthy controls from other groups. Serum AREG levels are higher in patients with persistent AF. These data suggested that EGF signaling pathway could be a therapeutic target for AF and serum AREG levels provide an effective biomarker for predicting persistent AF.

Atrial fibrillation (AF), the most prevalent cardiac arrhythmia, has an increasing prevalence worldwide. AF causes a severe medical condition requiring adequate treatment to prevent stroke or heart failure[1,2]. Recently, the role of inflammation in AF pathophysiology has gained increasing attention. Immune cells such as macrophages or T cells are markedly higher in the atria of patients with AF than in those of individuals with sinus rhythm and contribute to AF via electrical remodeling[3,4]. We have also demonstrated that circulating intermediate CD14^{++} CD16$^+$ monocytes are associated with AF onset and electrical and structural remodeling, suggesting the involvement of monocytes and macrophages in the pathogenesis of AF, although we could not reveal the information of atrial tissues[5,6]. Other

groups demonstrated that fibrosis, a consequence of inflammation, induces heterogeneous atrial depolarization, providing an opportunity for electrical disturbance[7–9]. These data suggested inflammation in AF, induced by immune cells, contribute to the pathophysiology of the condition of AF.

Recently, using single cell RNA-sequencing (scRNA-seq), SPP1$^+$ macrophages promote AF through cross-talk with stromal cells in patients with mitral regurgitation and persistent AF. Deleting SPP1 reduced AF incidence in a murine model with hypertension, obesity, and mitral valve regurgitation[10]. However, the mechanisms of inflammation at the single-cell level in patients with AF without underlying heart disease have not yet been clarified. Furthermore, although our understanding of AF mechanisms has

[1]Division of Cardiovascular Medicine, Department of Internal Medicine, Kobe University Graduate School of Medicine, Kobe, Japan. [2]Division of Cardiovascular Surgery, Department of Surgery, Yodogawa Christian Hospital, Osaka, Japan. [3]Department of Information and Intelligence Engineering, Kobe University, Kobe, Japan. [4]Division of Structural Medicine and Anatomy, Department of Physiology and Cell Biology, Kobe University Graduate School of Medicine, Kobe, Japan. [5]Division of Evidence-Based Laboratory Medicine, Kobe University Graduate School of Medicine, Kobe, Japan. [6]Division of Cardiovascular Surgery, Department of Surgery, Kobe University Graduate School of Medicine, Kobe, Japan. [7]Division of Cardiovascular Medicine, Department of Internal Medicine, Yodogawa Christian Hospital, Osaka, Japan. [8]Division of Cardiovascular Medicine, Department of Internal Medicine, Section of Arrhythmia, Kobe University Graduate School of Medicine, Kobe, Japan. [9]Division of Pharmacology, Kobe University Graduate School of Medicine, Kobe, Japan. [10]Division of Advanced Medical Science, Technology and Innovation, Kobe University Graduate School of Science, Kobe, Japan. ✉e-mail: emotot@med.kobe-u.ac.jp

greatly improved, it remains unclear how inflammation in AF is sustained and induces fibrosis. Single nucleus RNA-seq (snRNA-seq) is an alternative method to scRNA-seq for profiling gene expression of isolated nuclei instead of entire cells from frozen tissue; it is thus more appropriate to profile gene expression in cells that are challenging difficult to isolate. However, because snRNA-seq measures only transcripts pooled in nuclei, without cytoplasmic transcripts, it is unsuitable for detecting cellular activation in human immune cells such as microglia[11].

Therefore, we aimed to reveal the characteristic myeloid cell heterogeneity in left atrial (LA) tissue of patients with AF. We also aimed to elucidate the cell–cell interactions between myeloid and non-immune cells, using scRNA-seq for CD45+ immune cells and snRNA-seq for non-immune cells, to identify therapeutic targets for AF. In addition, we aimed to identify a potential biomarker for AF by investigating differences in gene expression profiles of macrophage populations between controls and patients with AF.

Results

scRNA- and snRNA-seq revealed the cell distribution in LA tissue of patients with AF and controls

SnRNA-seq from the frozen whole tissues identified 12 major cell types, and the data were analyzed via uniform manifold approximation and projection (UMAP) (Fig. 1C–E). Using canonical cell type markers, we identified fibroblasts (FBs), cardiomyocytes (CMs), myeloid cells, lymphoid cells, myeloid cell progenitors, endothelial cells (ECs), pericytes, myofibroblasts, adipocytes and neuronal cells (Fig. 1C–E). This clustering was consistent with the findings of previous studies describing the single-cell cardiac landscape[12,13].

In parallel with snRNA-seq, scRNA-seq from the sorted CD45+ immune cells were analyzed via UMAP to identify immune cell clusters. We used openly published datasets of single LA CD45+ cells from 4 samples obtained from 2 healthy donors (Human Cell Atlas Data Coordination Platform, accession ERP123138) to compare single-cell gene expression between control atrial tissue and that of patients with AF[14]. We first classified 13 clusters based on canonical immune cell markers. These 13 clusters comprised six clusters of myeloid cells (clusters 0–5), five clusters of T cells and natural killer cells (clusters 6–10), and three clusters of B cells (cluster 11–12) (Fig. 1F–H). The proportion of T cells and natural killer cells were higher in the AF group compared to controls. All cell clusters shown in Fig. 1 were consistently present across all samples in both scRNA-seq and snRNA-seq, as indicated in Supplementary Fig. 1A–D.

Five macrophage sub-clusters exhibited functional heterogeneity in LA tissue of patients with AF

We focused exclusively on the AF samples, rather than the controls, to explore the characteristics of myeloid cells in detail by integrating single-cell and histological data. The re-clustered myeloid cells were divided into five macrophage clusters [TNF+ (My.0), two IL1B+ (My.1 and My.4), TREM2+ (My.2), and LYVE1+ (My.3) resident macrophages]; three monocyte clusters [non-classical (My.5), classical (My.6), and ISG15+ monocytes (My.7)], five dendritic cell (DC) clusters (My.8–12), neutrophils (My.13), and mast cells (My.14) (Fig. 2A, left). Consecutively, the re-clustered UMAP highlighted distinct monocyte and macrophage sub-clusters because we want to focus on monocyte macrophage sub-clusters for the further analyses such as sc-Metabolism and RNA velocity (Fig. 2A right). My.0 cells were defined as TNF+ macrophages because of their high expression of inflammatory cytokines such as TNF, CCL3, and CCL4. Gene ontology (GO) analysis revealed that TNF+ macrophages (My.0) were enriched in 'human leukocyte antigen (HLA) class II protein complex binding' and 'immune receptor activity'. The gene expression pattern of TNF+ macrophages (My.0) was similar to that of TNF+ macrophages detected in coronary plaques[15]. My.1 and My.4, IL1B+ macrophages, exhibited high expression of proinflammatory cytokines IL1B and epidermal growth factor (EGF) ligand (AREG, EREG, and HBEGF) and THBS1. GO enrichment analysis revealed that the biological processes 'cell activation involved in immune response' and 'response to lipopolysaccharide'

were enriched in My.0, My.1, and My.4. However, the molecular functions 'glycosaminoglycan binding' and 'growth factor receptor binding' were enriched only in My.1 and My.4, but not in My.0 (Fig. 2A–D, Supplementary Fig. 2A, B). This suggests that IL1B+ macrophages (My.1 and My.4) have inflammatory and pro-fibrotic potential.

IL1B+ macrophages-2 (My.4) exhibited higher IL10, TIMP1, CLEC5A, VEGFA, and FN1 expression than IL1B+ macrophages-1 (My.1) (Fig. 2B, C, Supplementary Fig. 2B, D). Expression of these genes is associated with fibrosis. IL10 improves left ventricular function by ameliorating cardiac fibrosis after myocardial infarction[16]. TIMP1 is upregulated in chronic pressure-overloaded human hearts and is associated with the degree of interstitial fibrosis[17]. CLEC5A is associated with macrophage activation and the NLPP3 inflammasome[18,19]. VEGFA promotes AF by inducing inflammation-induced vascular leak[20]. Finally, FN1, associated with the extracellular matrix, is strongly associated with fibrosis[21,22].

My.2 cells exhibited high expression of TREM2 and CD9, pro-fibrotic markers in the liver[23]. TREM2, a cell surface lipid sensor that regulates phagocytosis in brain microglia[24], functions as a regulator of foamy macrophage differentiation and atherosclerotic plaque progression[25]. GO analysis has revealed enrichment of phospholipid binding enrichment, a molecular function. Although the function of TREM2+ macrophages (My.2) in the heart is unclear, it has been suggested that they function as anti-inflammatory pro-fibrotic macrophages during the late phase after myocardial infarction (Fig. 2A–D)[26].

My.3 is a LYVE1+ resident macrophage that uniquely expresses resident markers such as LYVE1 and FOLR2. GO enrichment analysis revealed that 'cardiac muscle tissue morphogenesis' and 'cargo receptor activity' were enriched in LYVE1+ resident macrophages (My.3) (Fig. 2D). LYVE1+ resident macrophages (My.3) selectively expressed MRC1, a scavenger receptor (Supplementary Fig. 2C). Metabolic pathway enrichment was evaluated using sc-Metabolism, a computational pipeline for quantifying metabolic change, using the scRNA-seq dataset to elucidate the metabolic landscape of each macrophage sub-cluster[27,28]: LYVE1+ resident macrophages (My.3) were less active in many metabolic pathways than other macrophage sub-clusters, and the glycolysis and gluconeogenesis pathways were suppressed only in LYVE1+ resident macrophages (My.3) (Fig. 2E). This suggests that LYVE1+ resident macrophages do not need extra energy and are metabolically stable.

Transmission electron microscopy (TEM) revealed at least two different types of macrophages or macrophage-like cells in LA tissue. One type of macrophage occurred alongside CMs and exhibited damaged mitochondria containing fewer cristae, suggesting that these macrophages take up dysfunctional mitochondria ("exophers") from neighboring CMs (Fig. 2Ha–d)[29]. The TEM images and scRNA-seq data support the hypothesis that LYVE1+ resident macrophages participate in cardiac homeostasis by regulating exophers; however, based on these findings, we cannot conclude that these TEM-identified macrophages are equivalent to LYVE1+ resident macrophages (My.3). The other type of macrophage or macrophage-like cell was located in interstitial tissue in the muscular layer (Fig. 2He) and the submucosa (Fig. 2Hf), surrounded by dense collagen fibers, recalling macrophages associated with fibrosis or myofibroblasts. These TEM images support the hypothesis that some macrophage sub-clusters, such as IL1B macrophages-1 (My.1), IL1B macrophages-2 (My.4), and TREM2 macrophages (My.2), are essential in inducing fibrosis.

My.5–7 were categorized as monocytes, as they were revealed to be major clusters in the Peripheral Blood Mononuclear Cells (PBMC) (Supplementary Fig. 2E). We utilized PBMC to clearly differentiate monocyte populations. Classical monocytes (My.6) exhibited higher CD14, VCAN, and LYZ expression but lower FCGR3A expression, whereas non-classical monocytes (My.5) exhibited lower CD14 expression but higher FCGR3A expression. My.7 was categorized as an ISG15+ monocyte because of its higher ISG15 expression, which is considered a typical response of classical monocytes to interferon stimulation[30]. ISG15+ monocytes were upregulated in the pressure-overloaded heart of a mouse model; this upregulation is related to adverse ventricular remodeling (Fig. 2A–C, Supplementary Fig. 2A)[31].
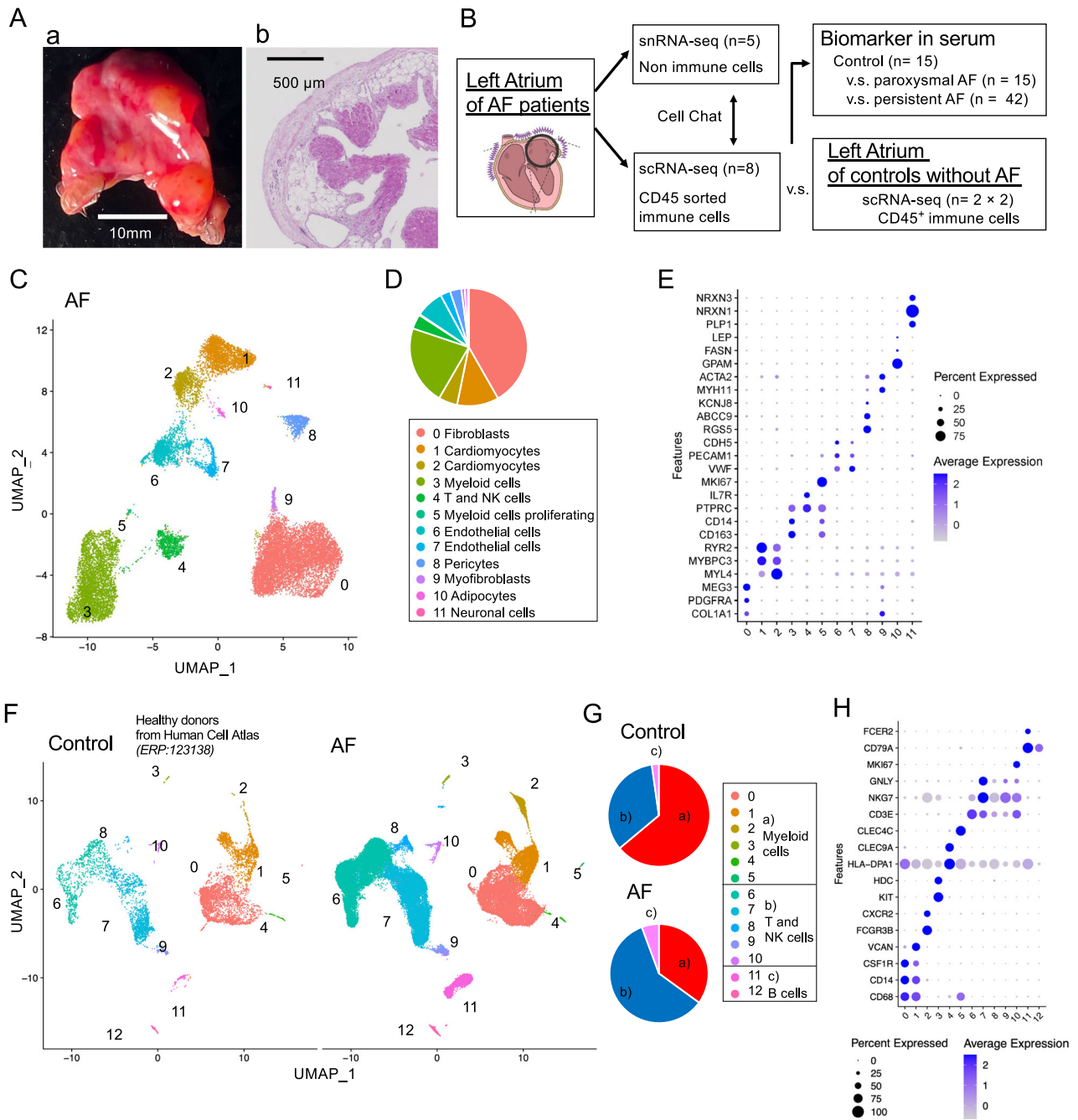
Fig. 1 | Cell landscape in left atrial (LA) tissues in atrial fibrillation (AF) and controls. A Representative LA sample obtained via LA appendectomy (**a**) and histology of LA tissue of patients with AF (hematoxylin and eosin staining) (**b**). **B** Scheme the study. SnRNA-seq ($n = 5$) and scRNA-seq ($n = 8$) data were obtained from LA tissue of patients with AF. Comparison of scRNA-seq data revealed the AF marker in serum. **C** Uniform manifold approximation and projection (UMAP) of all cells in LA tissue of patients with AF ($n = 5$). **C–E** are for LA tissue of patients with AF, analyzed by snRNA-seq. **D** Proportions of each cell type in LA tissue of patients with AF. **E** Dot plot displaying signature cell gene expression markers (SCGEMs) for each cell cluster. **F** UMAP of immune cells from 4 control LA tissue samples obtained from 2 sites of 2 donors (openly published datasets of healthy donors) and LA tissue of patients with AF ($n = 8$). **F–H** are for LA tissue of patients with healthy controls and AF, analyzed by scRNA-seq. **G** Proportions of each immune cell type in LA tissue of patients with AF and healthy controls: (**a**) Myeloid cells, (**b**) T and NK cells, and (**c**) B cells. **H** Dot plot displaying SCGEMs for each immune cell cluster in LA tissue of patients with healthy controls and AF.

My.8–12 were characterized as DCs owing to their elevated HLA expression (of genes such as *HLA-DR, HLA-DQ*, and *HLA-DP*), indicating their enhanced activation as antigen-presenting cells. Because My.8 and My.9 had higher *CLEC10A, CLEC4A*, and *CD1C* expressions than My.10–12, we categorized them as conventional DC2s. Moreover, unlike My.8, My.9 selectively expressed *PDGFB* and inflammatory genes (*TNF, CCL3*, and *CCL4*). Therefore, we identified My.9 as a *PDGFB*+ conventional DC2 and My.18 as a conventional DC2.

Owing to their selective *CLEC9A, IL3RA*, and *CCR7* expression, My.10–12 were categorized as conventional DC1s, plasmacytoid DCs, and mreg DCs, respectively. My.13 was categorized as a neutrophil because of its expression of neutrophil markers such as *FCGR3B* and *CSF3R*. My.14 was categorized as a mast cell, owing to its *KIT* and *HDC* expression (Fig. 2A–C, Supplementary Fig. 2A). All myeloid cell clusters were present in every sample, with the exception of neutrophils, as demonstrated in Supplementary Fig. 2A, F.
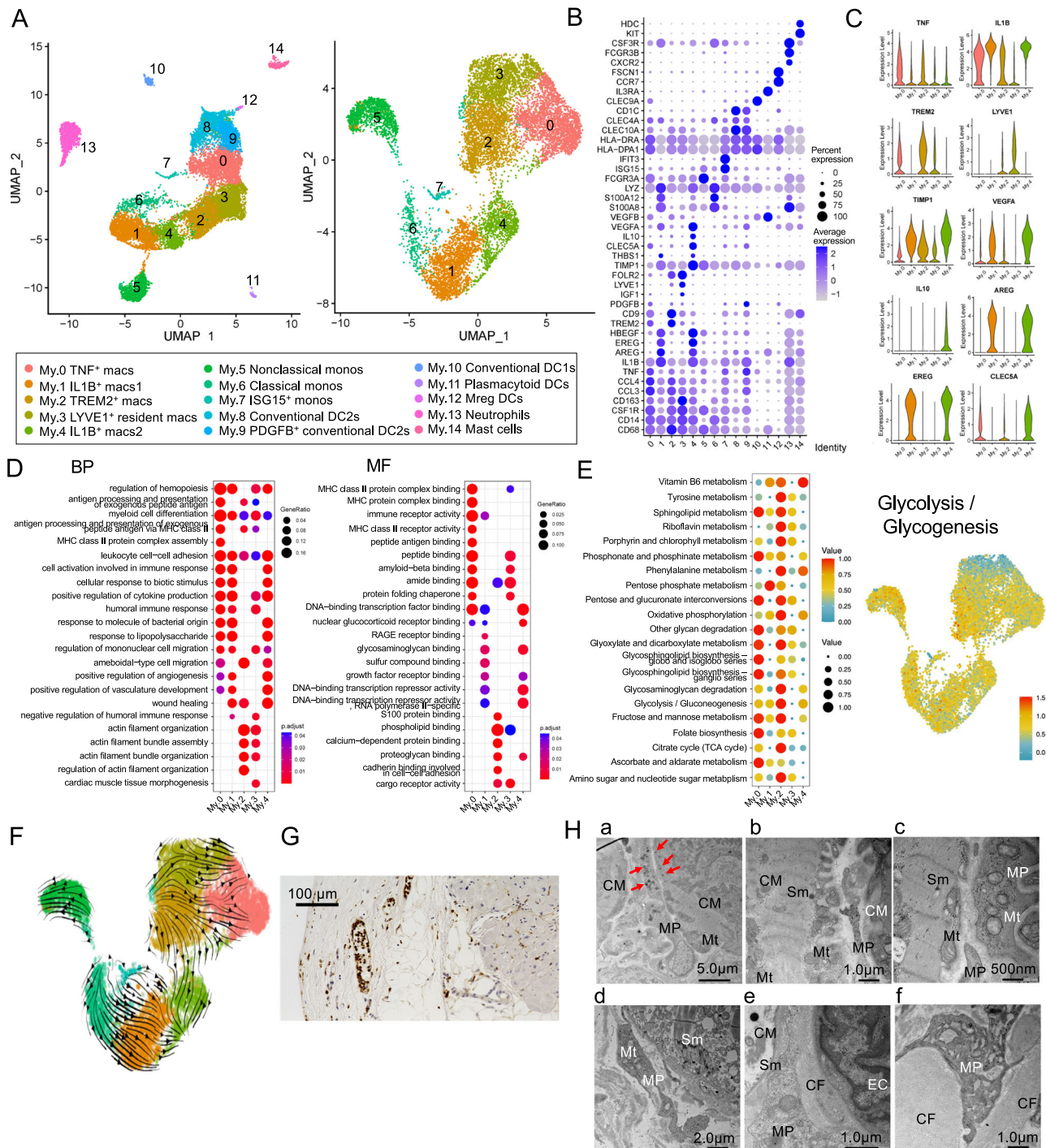
Fig. 2 | Left atrial (LA) myeloid cell immune landscape in atrial fibrillation (AF), analyzed by scRNA-seq. A Uniform manifold approximation and projection (UMAP) of all myeloid cells (left), and re-clustered UMAP focusing on macrophages and monocytes (right) in LA tissues of patients with AF ($n = 8$). macs, macrophages; monos, monocytes; DCs, dendritic cells. **B** Dot plot displaying signature cell gene expression markers (SCGEMs) for each myeloid cell cluster. **C** Violin plot displaying SCGEMs for each macrophage cluster. **D** Gene Ontology (GO) terms showing the enriched biological process (BP) and molecular function (MF) of each macrophage sub-cluster. **E** sc-Metabolism analysis revealing the enriched metabolic and glycolysis or gluconeogenesis pathways of each macrophage sub-cluster, following UMAP analysis of macrophages and monocytes (in LA of patients with AF). **F** Velocity field projected onto the UMAP plots of macrophages and monocytes in LA and of blood samples (patients with AF). **G** CD68 staining of LA tissue of patients with AF. **H** Transmission electron microscopy (TEM) images of LA samples (patients with AF) (**a–d**): macrophages absorbing dysfunctional mitochondria; macrophage-like cells in the interstitial tissue of the muscular layer (**e**) and sub-mucosa (**f**). CM, cardiomyocyte; MP, macrophage; CF, collagen fiber; Mt, mito-chondria; Sm, sarcomere; EC, endothelial cell. Red arrows indicated exophers.

RNA velocity, analyzed directly by distinguishing between un-spliced and spliced mRNAs[32], revealed that classical monocytes (My.6) differentiated into IL1B+ My.1 macrophages-1; IL1B+ macrophages-1 (My.1) and TREM2+ macrophages (My.2) differentiated into IL1B+ macrophages-2 (Fig. 2F); and TNF+ macrophages (My.0), for which few arrows were generated, did not differentiate into another phenotype. Histological CD68 staining supported these findings, indicating that classical monocytes in the small vessels located outside the heart were recruited to the cardiac tissue (Fig. 2G).

Myeloid cells signal FBs via the EGF and platelet-derived growth factor (PDGF) pathways

The re-clustered FBs were divided into five sub-clusters. FB.0 exhibited high expression of lipid-associated genes including *ABCA8* and *ABCA6*, suggesting that FB.0 facilitates cholesterol efflux[33]. GO analysis revealed ABC-type transporter activity enrichment (a biological process). FB.1 exhibited high expression of some fibrosis-related genes (*FBLN1, FBLN2, TIMP1, MMP2, COL3A1,* and *LUM*), while FB.3 exhibited high expression of others, including *ELN* and *FBN1*, suggesting that FB.1 and FB.3 were categorized as pro-fibrotic fibroblasts. GO analysis revealed that 'extracellular matrix/ structure/encapsulating structure organization' (a biological process) and 'collagen binding and integrin binding' (a molecular function) were upregulated in FB.1 and FB.3. Moreover, FB.4 cells were categorized as myofibroblasts because of their high expression of *ACTA2* and *MYH11*, associated with muscle contraction. FB.2 exhibited high expression of inflammation-associated genes such as *CCL2* and *EGR1*. GO enrichment analysis revealed enrichment of 'response to fibroblast growth factor' and 'myeloid leukocyte differentiation' (biological processes) in FB.1, suggesting that FB.2 participates in inflammatory processes (Fig. 3A, B, Supplementary Figs. 3A and 4A).

We applied Cell-Chat analysis to identify interactions between myeloid cells and FBs[34]. IL1B+ macrophages-1 (My.1) and macrophages-2 (My.4) send EGF signals to FBs (especially FB.1 and FB.2). The expressions of EGFR, ERBB2 and ERBB4, receptors for EGF signaling, were plotted on the UMAP (Supplementary Fig. 5A).

PDGFB+ conventional DC2s (My.9) and TNF+ macrophages (My.0) send PDGF signals to FBs. In a rat AF model, PDGF-B promoted the proliferation and COL1 secretion of atrial fibroblasts[35]. Conversely, FBs (especially FB.1 and FB.4) send FN1 and COLLAGEN signals to IL1B+ macrophages-1 and 2 (My.1 and My.4), suggesting a positive feedback loop in the interaction between myeloid cell and FBs[36,37]. It was unclear how IL1 and SPP signaling occurred between myeloid cells and FBs; however, a previous study has demonstrated that SPP1 macrophages promote AF through cross-talk with local immune and stromal cells (Fig. 3C, Supplementary Fig. 3B)[10].

Myeloid cells signal ECs via the VEFG and IL1 pathways

The re-clustered ECs were divided into five sub-clusters. EC.0 and EC.1 were defined as capillary ECs, owing to their high expression of *RGCC* and *CA4*, capillary marker genes. EC.0 exhibited higher expression of angiogenesis-related genes such as *NOTCH4, EGFL7,* and *ITGA6* than EC.1. EC.2 cells were defined as venous ECs because of their high expression of venous EC markers such as *ACKR, NR2F2,* and *VCAM1*[38]. EC.2 exhibited high expression of inflammatory-related genes such as *CXCL2, TLR4,* and *EGR1* and *ACKR1*, which regulates leukocyte recruitment[39]. EC.3 exhibited high expression of the endocardial marker genes *SMOC1* and *NPR3*[40,41]. EC.4 cells were defined as arterial ECs because of their high expression of arterial marker genes such as *SEMA3G* and *EFNB2*[14]. EC.4 also expressed *ADAMTS1* and *THBD*, associated with thrombosis in AF[42]. Therefore, EC.4 could be a target to prevent thrombosis formation (Fig. 3D, E, Supplementary Figs. 3C and 4B).

We further investigated the interaction between myeloid cells and ECs through Cell-Chat analysis. IL1B+ macrophages-1 and 2 (My.1 and 4) send vascular endothelial growth factor (VEGF) signals to ECs (especially EC.0). EC.4 sends NOTCH signals to EC.0 and myeloid cells primarily IL1B+ macrophages-1 (My.1). The notch signaling pathway promotes macrophage differentiation and inflammation[43]. IL1B+ macrophages-1 and 2 (My.1 and My.4) send IL1 signals to ECs (especially EC.3). Cell-Chat analysis revealed that LYVE1+ resident macrophages (My.3) send Insulin-like Growth Factor 1 (IGF-1) signals to ECs (EC.0, EC.2, and EC.4) (Fig. 3F).

Myeloid cells signal CMs via the IGF and EGF pathways

The re-clustered CMs were divided into three sub-clusters. Levels of typical atrial CM markers (*NPPA* and *MYH6*) were higher in cluster 1 (CM.1) than

in CM.0 or CM.2[14]. CM.2 exhibited high expression of *SORBS2*, associated with reduced cardiomyocyte contraction and Ca^{2+} handling activity in left ventricular noncompaction cardiomyopathy (Fig. 3G, H)[44]. Consistent with a prior of single-cell LA data[33], CM.2 may be a pathological myocardial sub-cluster associated with AF.

We investigated the interaction between myeloid cells and CMs using Cell-Chat analysis. LYVE1+ resident macrophages (My.3) send IGF signals to SORBS2+ cardiomyocytes (CM.2). IL1B+ macrophages-1 (My.1) and IL1B+ macrophages-2 (My.4) send EGF signals to SORBS2+ cardiomyocytes (CM.2). In addition to the effect of IGF-1 on ECs, IGF-1 also mediates adaptive cardiac growth during hypertension[45]. We suspect that LYVE1+ resident macrophages (My.3) may rescue SORBS2+-damaged CMs (CM.2) via the IGF-1 pathway (Fig. 3I). The expressions of IGF1R, IGF2R, ITGB3, ITGB4, ITGAV, which are receptors for IGF signaling, were plotted on the UMAP (Supplementary Fig. 5B).

Monocyte and macrophage characteristics in AF reveal serum amphiregulin as an AF biomarker

We compare single-cell monocyte and macrophage gene expression between control atrial tissue and that of patients with AF[14]. An integrated UMAP was generated by combining atrial tissue from healthy controls and from patients with AF (Fig. 4A, Supplementary Fig. 6A). The proportion of LYVE1+ resident macrophages (My.3) tended to be smaller in the AF group than in the control group (Fig. 4B). LYVE1+ resident macrophages (My.3) specifically expressed IGF-1 in both the control and AF groups (Supplementary Fig. 4D).

Because of the functional importance of IGF-1[45], we tested whether circulating IGF-1 levels could be a surrogate marker for AF. Controls were recruited from patients with paroxysmal supraventricular tachycardia who needed catheter ablation. We compared circulating IGF-1 levels in serum between controls, patients with paroxysmal AF, and patients with persistent AF. Patient characteristics are presented in Table 2. Serum IGF-1 levels were tended to be reduced in patients with paroxysmal AF and were significantly reduced in patients with persistent AF (Supplementary Fig. 6E). Although aging affected circulating IGF-1 levels, logistic regression analysis identified IGF-1 as an independent predictor of AF presence, but not of persistent AF (Supplementary Table 1). While the percentage of IGF-1 positive cells with expression levels over 1.0 in the myeloid cell cluster were reduced in AF (6.61% vs 5.79%), IGF-1 expression levels in resident macrophages (My.3) were higher in AF (Supplementary Fig. 6D). IGF-1 was expressed in both the myeloid and fibroblast cell clusters in snRNA-seq data (Supplementary Fig. 6F, G).

The velocity analysis revealed that IL1B+ macrophages-1 (My.1) are derived from classical monocytes (My.6) (Fig. 2F). We therefore present a volcano plot illustrating the differential expression of genes in classical monocytes (My.6) and monocyte-derived IL1B+ macrophages-1 (My.1), comparing the control and AF groups. *AREG* was one the most upregulated genes in the AF group (Fig. 4C). AREG is an EGF ligand in a crucial signaling pathway between myeloid cells and FBs (Fig. 3C); we therefore focused on it for further analyses. *AREG* expression in IL1B+ macrophages-1 (My.1), IL1B+ macrophages-2 (My.4), and classical monocytes (My.6) was significantly higher in the AF group than in the control group (Fig. 4D, E). AREG is primarily expressed in the myeloid cell cluster in scRNA-seq data. However, its expression was not detected in the snRNA-seq data, even within the macrophage cluster. This suggests that the snRNA-seq method might have limitations in detecting certain genes, including AREG (Supplementary Fig. 6F, G).

Therefore, to test whether AREG could be a surrogate biomarker, we compared circulating serum AREG levels in the same cohort used to examine IGF-1 levels. Serum AREG levels were elevated in patients with persistent AF but not in controls: 35.7% (15/42) of patients with persistent AF, but none of the controls, exhibited elevated serum AREG (Fig. 4F, G). Given that EREG and HBEGF also function as EGF ligands, we analyzed their gene expression: *EREG* and *HBEGF*
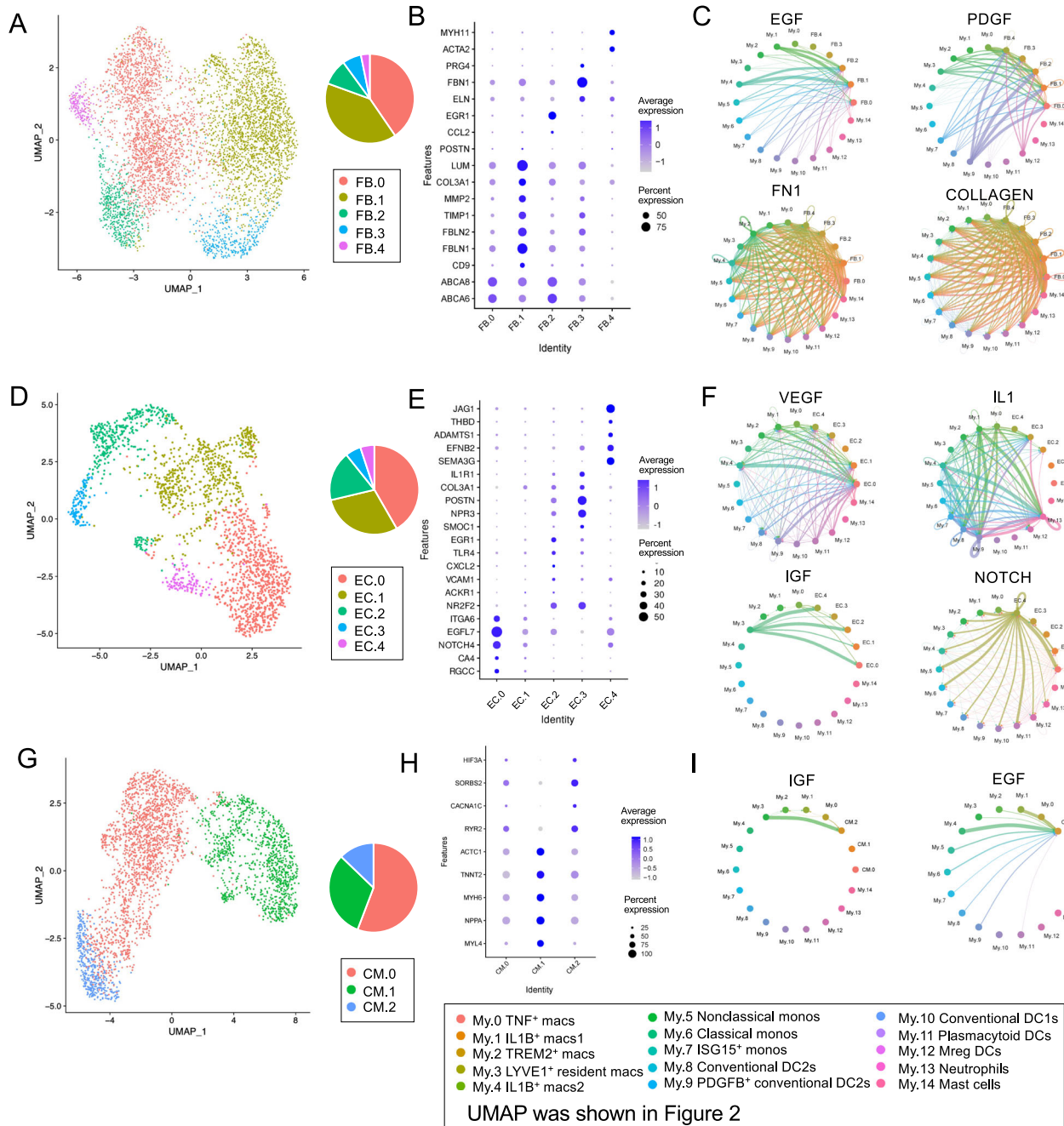
Fig. 3 | Left atrial (LA) non-immune cell landscape in atrial fibrillation (AF); the interactions between non-immune cells (snRNA-seq data) and myeloid cells (scRNA-seq data). **A** Uniform manifold approximation and projection (UMAP) of fibroblasts (FBs) in the left atria (LA) of patients with atrial fibrillation (AF) (*n* = 5). Proportions of each FB sub-cluster. **B** Dot plot displaying signature cell gene expression markers for each FB cluster. **C** Cell-Chat analysis of EGF, PDGF, FN1, and COLLAGEN interactions between myeloid cells and FBs. **D** UMAP of endothelial cells (ECs) in LA (patients with AF) (*n* = 5). Proportions of each EC sub-cluster. **E** Dot plot displaying SCGEMs for each EC cluster. **F** Cell-Chat analysis of VEGF, IL1, IGF, and NOTCH interactions between myeloid and ECs. **G** UMAP of cardiomyocytes (CMs) in LA (patients with AF) (*n* = 5). Proportions of each CM sub-cluster. **H** Dot plot displaying signature cell gene expression markers for each CM cluster. **I** Cell-Chat analysis of IGF and EGF interactions between myeloid cells and CMs.

expression in IL1B$^+$ macrophages-1, IL1B$^+$ macrophages-2, and classical monocytes, were higher in the AF group than in the control group (Supplementary Fig. 6B, C). Finally, we used openly published datasets of single LA nuclei obtained from 14 healthy donors (Human Cell Atlas Data Coordination Platform, accession ERP123138) to compare single-nucleus fibroblast gene expression between control atrial tissue and that of patients with AF[40]. An integrated UMAP demonstrated the proportion of fibroblasts (No.1 and 2) were detected only in the AF group, suggesting the phenotypic change of fibroblasts in AF (Supplementary Fig. 7A–C).

Discussion

For patients with AF, we examined myeloid cell heterogeneity of LA tissue, and the cell–cell interactions between myeloid and non-immune cells, via scRNA-seq for CD45$^+$ immune cells and snRNA-seq for non-immune cells. ScRNA-seq can be used to analyze all RNAs in the cytoplasm and nucleus, providing a major advantage, especially for immune cells. Conversely, snRNA-seq enables the detection of all cell types in the heart. We also used openly published datasets of single LA CD45$^+$ cells from healthy donors to identify the specific cell population and gene expression in AF. Serum AREG was identified as a biomarker for AF.
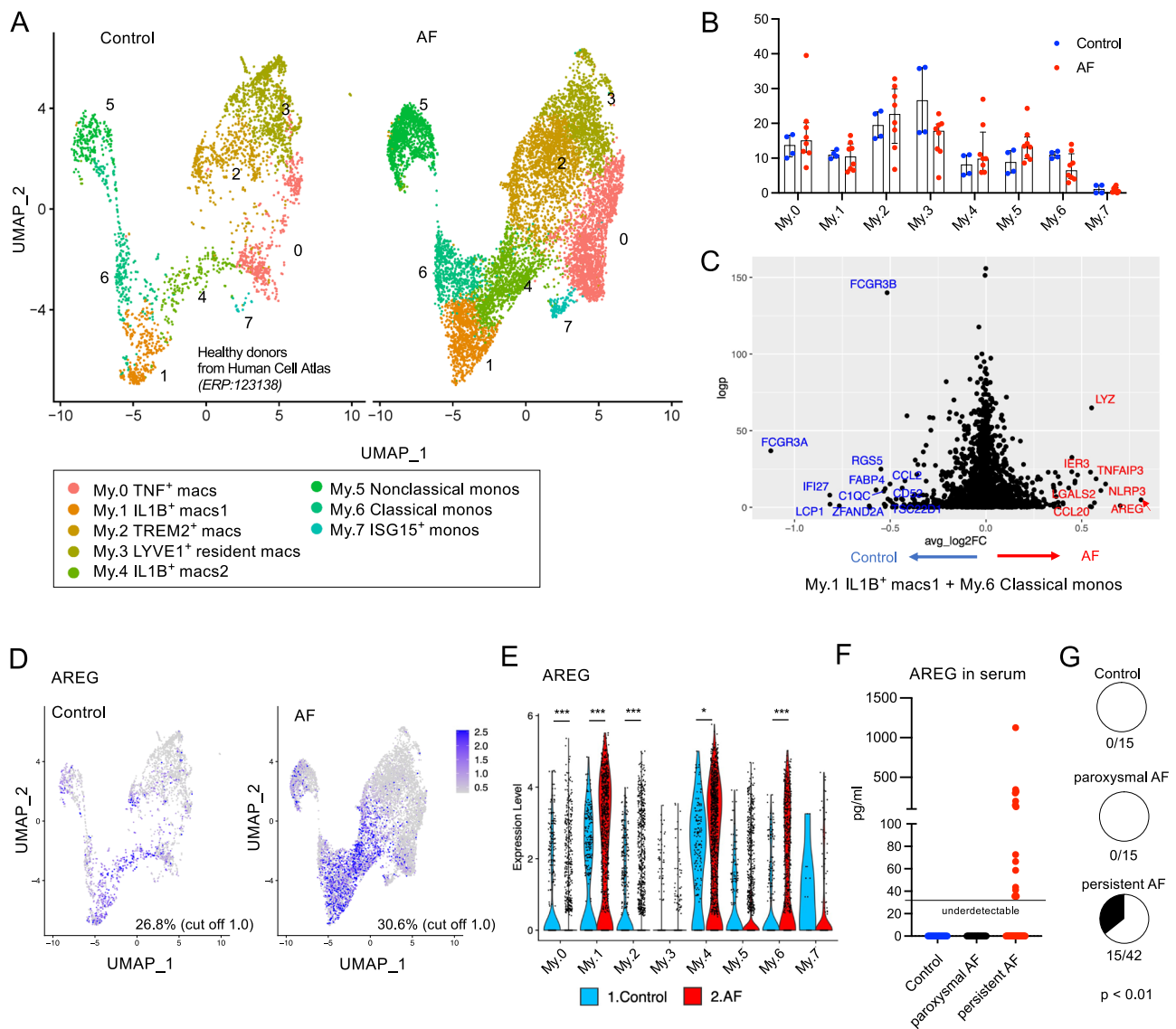
Fig. 4 | Macrophages and monocytes in controls and atrial fibrillation (AF) groups, analyzed by scRNA-seq. A Uniform manifold approximation and projection (UMAP) of macrophages and monocytes in from 4 control samples obtained from 2 sites of 2 donors (openly published datasets of healthy donors) and AF groups. macs, macrophages; monos, monocytes. **B** Proportions of each macrophage and monocyte sub-cluster in the control (blue) and AF groups (red). Data were expressed as median with interquartile range and compared using Wilcoxon rank-sum testing. **C** A volcano plot of genes in IL1B+ macrophages-1 (My.1) and non-classical monocytes (My.6) exhibiting differential expression between the control and AF groups (non-parametric Wilcoxon rank sum testing). Blue: upregulated in controls; red: upregulated in AF samples. The thresholds were $\log(p) > 10.0$ and average $\log_2$(fold change) > 0.5 (for AF samples) or $\log_2$(fold change) < −0.5 (for controls). **D** Feature plot of AREG expression in macrophages and monocytes. **E** AREG expression in each macrophage and monocyte sub-cluster (scRNA-seq data). Wilcoxon rank-sum testing. **F** Circulating serum AREG levels ($n = 15$ vs 15 vs 42). Kruskal−Wallis testing followed by Dunn's post hoc analysis. **G** Proportions of AREG-positive patients (n: 15 for controls, 15 for paroxysmal AF, and 42 for persistent AF). Chi-square testing. Statistical significance was expressed as $*p < 0.05$, $**p < 0.01$, or $***p < 0.001$.

Cardiac macrophages can be classified into resident and recruited monocyte-derived macrophages, derived from embryonic and hematopoietic origins, respectively[46]. Cardiac resident macrophages maintain cardiac mitochondrial homeostasis in a steady state via tyrosine–protein kinase MER-mediated phagocytosis of dysfunctional mitochondria[29]. These macrophages regulate tissue-reparative activities after myocardial injury[47] and play key roles in stimulating angiogenesis and inhibiting cardiac fibrosis[46]. Although resident macrophages constitute the main macrophage population in healthy hearts, recruited monocyte-derived macrophages become dominant in diseased hearts, such as in dilated cardiomyopathy or myocardial infarction[48,49]. Our results for AF reveal the same tendency as that observed in other types of heart disease, namely an elevated proportion of monocyte-derived IL1B+ macrophages and a reduced proportion of LYVE1+ resident macrophages. Furthermore, for the first time, we succeeded in capturing TEM images of tissue-maintaining macrophages in LA taking up dysfunctional mitochondria (i.e., "exophers") from neighboring CMs. The TEM images and scRNA-seq data support the hypothesis that LYVE1+ resident macrophages participate in cardiac homeostasis by regulating exophers. However, based on these findings, we could not conclude that the macrophages observed using TEM were equivalent to the LYVE1+ resident macrophages characterized using scRNA-seq.

Cardiac resident macrophages have an anti-fibrotic function[46]. Our findings reveal that LYVE1+ resident macrophages selectively express IGF-1 and signal ECs and SORBS2+ CMs via the IGF-1–IGF-1 receptor pathway. We hypothesize that LYVE1+ resident macrophages (My.3) may rescue damaged SORBS2+ CMs (CM.2) via the IGF-1 pathway, based on prior

studies revealing that IGF-1 drives compensatory cardiac muscle growth in hypertension[45]. Because IGF-1 increases nitric oxide production in ECs[50], LYVE1^{+} resident macrophages (My.3) may play a protective role against endothelial dysfunction by sending IGF-1 to ECs. Although circulating IGF-1 is primarily derived from the liver and exhibits endocrine activity, IGF-1 can also be secreted by other tissues or immune cells, acting locally and exerting a paracrine function[51]. It remains unclear how circulating IGF-1 and local IGF-1 from LYVE1^{+} resident macrophages (My.3) differ in their effects; nonetheless, based on our findings, we suspect that cross-linking occurs between local and circulating IGF-1. These findings identify circulating serum IGF-1 levels as a surrogate marker for the presence of AF, although IGF-1 expression level in resident macrophages (My.3) were significantly higher in AF. This discrepancy indicates that it is difficult to conclude that IGF-1 is fully compatible with the serum data. Busch et al.[52] have reported that IGF-1 is associated with AF, in a population-based study, providing support for our results. Increasing clinical evidence indicates the involvement of the IGF-1 axis in pleiotropic responses elicited by sodium-glucose transporter-2 inhibitors[53]. There is a need for IGF-1-based approaches for treating cardiovascular diseases, including AF.

In contrast, following cardiac-pressure overload, monocyte-derived macrophage recruitment aggravated fibrosis, and classical monocyte influx into LA tissue causes persistent inflammation in AF[46,54]. Here, the velocity analysis and histological assessment suggested that classical monocytes infiltrated from the outside of the heart and transformed into IL1B^{+} macrophages. Notably, classical and non-classical monocytes were detected in the LA tissue. We have previously demonstrated that circulating intermediate CD14^{++} CD16^{+} monocytes are associated with AF onset[5,6]. Together, these prior and current findings suggest that non-classical monocytes, including CD14^{++} CD16^{+} and CD14^{+} CD16^{++} monocytes, may have a crucial function in AF.

In mice, inflammatory macrophage-derived IL1B prolongs the action potential duration, reduces K^{+} and L-type Ca^{2+} currents, and increases susceptibility to arrhythmia[55,56]. Moreover, inhibiting the IL1 receptor increases the conduction velocity and improves spontaneous and inducible ventricular arrhythmias[57]. Although canakinumab, a therapeutic monoclonal antibody targeting IL1B, reduced the six-month recurrence rate of AF, the reduction was not significant owing to the limited sample size[58].

AREG expression was significantly higher in AF samples than in controls for classical monocytes, IL1B^{+} macrophages-1 and -2, suggesting AREG is a potential novel therapeutic target for AF. AREG is crucial for wound healing and various aspects of tumorigenesis metastasis and has gained increasing attention owing to its pro-fibrotic function in multiple organs such as the lungs, kidneys, and liver[59–63]. For example, AREG promotes bleomycin-induced pulmonary fibrosis by activating fibroblasts or inducing differentiation into myofibroblasts[60] and contributes to airway remodeling in chronic allograft dysfunction in the lungs[63]. AREG is distinct from other EGF ligands in that it can induce a mitogenic signal and cell differentiation. The weak stability of the AREG explains this observation; EGFR binding, which cannot induce receptor internalization, enables AREG to induce a sustained signal downstream of the receptor and cell differentiation[64]. We suspect that TREM2^{+} macrophages and IL1B^{+} macrophages-1 and -2 function as pro-fibrotic macrophages. Especially, IL1B^{+} macrophages-2 (My.4) exhibited higher *IL10, TIMP1, CLEC5A, VEGFA*, and *FN1* expression than IL1B^{+} macrophages-1, suggesting IL1B^{+} macrophages-2, mostly differentiated from TREM2^{+} macrophages, were suspected to be more pro-fibrotic than the other two macrophages.

In contrast, cardiac macrophage-derived AREG improves gap junction activity and prevents lethal arrhythmia in CMs at the right ventricle[65]. Nonetheless, we cannot yet clearly reconcile our findings with those of prior studies. Although the function of AREG in the heart and in AF remains unclear, our data support the hypothesis that AREG induces fibrosis via EGF receptor signaling in FBs in patients with AF. Consistent with our findings, genetic variants in the gene locus of the EGF receptor are associated with AF progression[66]. Although our study did not include control samples from participants without AF, it reveals, for the first time, that circulating AREG levels were upregulated in persistent AF, using samples from

different patients, thereby validating our scRNA-seq findings and compensating for the lack of controls in the scRNA-seq analysis. In future, the function of AREG in AF should be clarified in a murine model. AREG-targeting self-assembled-micelle inhibitory RNA is clinically effective against fibrosis, by stably silencing *AREG*[62]. The scRNA-seq and serum data presented here reveal IGF-1 and AREG as important functional biomarkers and therapeutic targets to prevent fibrosis progression in AF.

This study has several limitations. First, the sample size was small, which prevented us from evaluating the impact of individual patient backgrounds on the study results. Second, our analysis focused on LA appendages obtained via LA appendectomy. Consequently, we could not investigate the initiation of ectopic beats, as pulmonary veins—key sources of ectopic beats that frequently trigger paroxysms in AF—were not sampled[67]. Third, we did not include own control samples of patients without AF. Fourth, we did not provide spatial histological staining for AREG expression.

In conclusion, we characterize the myeloid cell heterogeneity of LA tissue in patients with AF and the cell–cell interactions between myeloid and non-immune cells. Classical monocytes and inflammatory macrophages were found to send EGF signals to FBs. AREG were identified as a potential functional biomarker and a therapeutic target for AF.

Methods
Patients recruitment
LA tissues were obtained from nine patients with AF who underwent LA appendectomies, which was offered to patients who had high thromboembolic and bleeding risks. To construct scRNA-seq libraries, sorted CD45^{+} immune cells from eight patients with AF were applied to a 10X platform. To construct snRNA-seq libraries, LA tissue was collected and frozen after collection from five patients with AF and were applied to a 10X platform. LA tissue from four patients was used for both scRNA- and snRNA-seq libraries. All ethical regulations relevant to research participants were followed. All participants provided written informed consent upon enrollment. The study was approved by the Ethics Committees of Kobe University and Yodogawa Christian Hospital and registered with the UMIN Clinical Trials Registry (000047006). A representative overall image acquired via LA appendectomy (Fig. 1Aa) and a histological image of the LA sample stained with hematoxylin and eosin (Fig. 1Ab) is presented. The strategy for this project is described in Fig. 1B. Patient characteristics are presented in Tables 1 and 2. The investigation of biomarkers was approved by the local ethics committee of Kobe University and registered with the UMIN Clinical Trials Registry (UMIN ID: 000030297).

Histology
LA samples extracted by LA appendectomy were immediately fixed with Paraformaldehyde, 4% in PBS. Tissue specimens were processed with a paraffin embedding system. LA sections were cut into a thickness of 4 μm, mounted on slides, and stained with Hematoxylin and Eosin, Masson's trichrome. For immunohistochemistry, LA sections were incubated with the primary antibodies to CD68 (1:500, Agilent Technologies, M0814) overnight at 4 °C, followed by the HRP conjugated anti-mouse IgG(H + L) goat polyclonal secondary antibody (HISOFINE #424134; Nichirei Bioscience, Tokyo, Japan) for 30 min at room temperature. The staining was visualized using 3,3′-diaminobenzidine, tetra-hydrochloride (DAB) (Genemed Bio-technologies, 10-0048). Nuclear was identified with Mayer's hematoxylin.

All-in-one–type fluorescence microscope (BZ-X700; Keyence) were used for observation of stained sections.

Transmission electron microscopy (TEM)
LA samples were dissected and fixed with 2.5% glutaraldehyde in 0.1 M phosphate buffer and then treated with 1% to 2% OsO4 in 0.1 M phosphate buffer for 1 to 2 h. After dehydration with a graded series of ethanol solutions, the tissues were embedded in epoxy resin. Ultrathin sections with a thickness of 100 nm were prepared using an ultramicrotome (ULTRACUT S, Leica), stained with EM stainer (Nissin EM) and lead stain solution (Sigma). Sections were visualized by a transmission electron microscope JEM 1400-Plus (JEOL).

Table 1 | Baseline characteristics of study participants for scRNA-seq and snRNAseq

Patients Sample no Nuclei or Cell	P1 LA6 (cell) LA1or2 (nuclei)	P2 LA7 (cell) LA1or2 (nuclei)	P3 LA8 (cell) LA1or2 (nuclei)	P4 LA9 (cell)	P5 LA10 (cell) LA5 (nuclei)	P6 LA11 (cell) LA3or4 (nuclei)	P7 LA12 (cell)	P8 LA13 (cell)	P9 LA3or4 (nuclei)
Characteristics									
AF duration (months)	6	11	9	120	240	360	240	120	120
Age	41	64	76	75	79	70	72	62	80
Sex	F	M	F	M	M	M	M	M	M
BMI (kg/m^2)	27.1	22.5	24.3	29.8	24	25.2	20.8	26.1	25.9
History of smoking	−	+	+	+	+	+	−	+	−
Stroke	+	−	+	+	−	+	−	−	+
Bleeding	−	−	+	−	+	−	−	−	+
Hypertension	−	+	+	+	+	+	+	−	+
Diabetes	−	+	+	+	−	−	−	−	−
Dyslipidemia	−	−	−	+	−	−	+	+	−
Medications									
Anticoagulant	Dab	War	Api	Riv	Api	Dab	Api	Riv	Edo
Antiplatelet drug	−	−	−	−	−	−	−	+	−
Antiarrhythmia drug	−	−	−	−	−	−	+	−	+
β-blocker	+	−	−	−	−	+	−	+	+
Ca blocker	−	−	−	+	−	−	+	+	−
Echocardiogram									
LVEF (%)	57	50	60	60	61	65	68	46	55
LA diameter (mm)	44	51	40	58	59	63	56	52	59

AF atrial fibrillation, *BMI* body mass index, *LA* left atrium, *LVEF* left ventricular ejection fraction, *Dab* dabigatoran, *Warf* warfarin, *Api* Apixaban, *Riv* rivaroxaban, *Edo* Edoxaban.

Table 2 | Baseline characteristics of study participants for ELISA measurement of circulating Amphiregulin (Areg) and Insulin-like growth factor-1 (IGF-1)

	Control (*n* = 15)	Paroxysmal AF (*n* = 15)	Persistent AF (*n* = 42)
Male, *n* (%)	5 (33.3)	8 (53.3)	37 (88.0)
Height (m)	1.64 ± 0.08	1.65 ± 0.12	1.68 ± 0.09
Weight (kg)	62.4 ± 14.4	64.5 ± 11.2	66.9 ± 12.6
BMI (kg/m^2)	23.0 ± 3.6	23.5 ± 1.9	24.3 ± 3.6
Age (years old)	44 (27–50)	60 (50–75)	68.5 (58–74)
BNP (pg/ml)	10.9 (7.1–15.7)	10.4 (5.7–48.8)	60 (40.8–186.2)
Creatinine (mg/dL)	0.73 (0.62–0.83)	0.95 (0.89–0.99)	0.82 (0.74–1.01)
AST (U/L)	19 (18–24)	23 (17–27)	23.5 (18.8–28)
ALT (U/L)	15 (11–32)	15 (11–17)	20 (16–28)
LAD (mm)	29.0 ± 4.8	33.5 ± 4.7	41.3 ± 6.3
LVEF (%)	63.5 (57.6–66.5)	62.8 (58.6–66.1)	58.4 (52.8–62.2)

BMI body mass index, *BNP* brain natriuretic peptide, *AST* aspartate aminotransferase, *ALT* alanine aminotransferase, *LA* left atrium, *LVEF* left ventricular ejection fraction.

Preparation for scRNA-seq

LA samples were immediately stored in Tissue Storage Solution (Miltenyi Biotec, 130-100-008) after collection at an operating room and transferred to the laboratory and processed within 8 h. Each sample was washed, chopped into small pieces, and digested in enzymatic digestion buffer with 450 U/ml collagenase I (Sigma, C0130), 125 U/ml collagenase XI (Sigma, C7657), 60 U/ml DNase I (Roche, 04536282001) and 60 U/ml hyaluronidase (Sigma, H3506) at 37 °C for 30 min while shaking. The digested samples were filtered through 40-µm cell strainers (BD, 352340), washed, centrifuged at 300 *g* for 10 min. Digested cells from LA samples were washed wish presort buffer (BD, 563503) and stained with Fc-block (Human TruStain FcX™, Biolegend, 422302) for 10 min, PE/Cyanine7 anti-human CD45 Antibody (Biolegend, 368532) for 30 min and 7AAD (BD, 559925) for 10 min. Fluorescence activated live CD45+ cells were sorted by flow cytometry using the BD Biosciences FACSAriaIII and immediately applied to the next step of the single-cell sequencing library preparation within 24 h after sample collection.

Preparation for snRNA-seq

Each sample was cut into small pieces and frozen into liquid nitrogen. Nuclei isolation was performed according to Chromium Nuclei Isolation Kit with RNase Inhibitor (PN-1000494). Frozen tissue samples are homogenized with a pestle in Lysis Buffer and passed through a column. Next, debris is removed via centrifugation in Debris Removal Buffer. The isolated nuclei are then washed and resuspended and loaded directly into compatible 10x Genomics protocol for making libraries.

Peripheral blood mononuclear cell

Fresh peripheral blood samples of patients with atrial fibrillation (AF) were obtained in ethylenediaminetetraacetic acid-coated tubes just before operation on the day of left atrial appendectomy. Immediately after collecting the blood samples, peripheral blood mononuclear cells (PBMCs) were isolated by Ficoll gradient centrifugation.

Fluorescence activated cell sorting

Digested cells from LA samples or PBMCs were washed wish presort buffer (BD, 563503) and stained with Fc-block (Human TruStain FcX™, Biolegend, 422302) for 10 min, PE/Cyanine7 anti-human CD45 Antibody (Biolegend, 368532) for 30 min and 7AAD (BD, 559925) for 10 min. Fluorescence activated live CD45$^+$ cells were sorted by flow cytometry using the BD Biosciences FACSAriaIII and immediately applied to the next step of the single-cell sequencing library preparation.

Library preparation for scRNA-seq and snRNA-seq

Single cell sequencing libraries were prepared as outlined in the 10x Genomics Single Cell 3′ Reagent Kits v3.1 or 5′ Reagent Kits v2 user guide. Before loading onto the 10x Genomics single-cell-A chip, the cell concentration was adjusted to reach the required cell concentration according to the user guide by pelleting and re-suspending the samples. The cell suspensions were loaded onto a Chromium single-cell chip along with partitioning oil, reverse transcription (RT) reagents, and a collection of gel beads that contained unique 10X barcodes.

After the preparation of single-cell gel bead-in-emulsions, reverse transcription (RT) was performed using a Thermal Cycler (Thermo Fisher Scientific). Samples were diluted and run on a Bioanalyzer (Agilent Technologies) to determine the concentration of cDNA. 10x Genomics 3′ Cell-Plex Kit (10X Genomics, 1000261) was used to differentiate between blood and atrial tissues.

The amplified cDNA was purified by using SPRI select magnetic beads (Beckman Coulter). Single cell libraries were then constructed by fragmentation, end repair, polyA tailing, adaptor ligation, and size selection based on the manufacturer's standard parameters. Each sequencing library was created with a unique sample index.

Data processing of scRNA-seq and snRNA-seq

Samples were sequenced by using an Illumina NovaSeq 6000 a read depth of ~50,000 reads/cell The sequenced data were processed into expression matrices with the Cell Ranger Single Cell Software (v 6.1.2) of 10X Genomics against the GRCh38 human reference genome with default parameter. Raw base call file from Novaseq sequencer were demultiplexed into FASTQ files for each library. Analyses were performed using Seurat (v.4.1.1) in an R 4.2.1 environment[68]. Before processing, reads were filtered to remove mitochondrial genes. To exclude doublets and low-quality cells, only cells expressing between 500 and 5000 genes and less than 8% mitochondrial genes and genes expressed in at least 3 cells were used for further analyses. For the visualization of the cells in a two- dimensional space, we performed a principal component analysis on the integrated dataset and used the first 10–30 principal components (PCs) for UMAP. We assessed differential gene expression using non-parameteric Wilcoxon rank sum test implemented by Seurat FindMarkers function. Top 10 unique differentially expressed genes in each cluster were identified by testing gene expression between each cluster and all other clusters combined and shown as heatmaps. Dotplot was performed to identify each cluster based on the unique differentially expressed genes or the expression of the known canonical marker genes. Batch effects were corrected using Seurat integration with the "rpca" method. After the selection, Log-normalized with the default parameters.

We clustered all the cells based on the integrated gene expression matrix using Seurat with a parameter resolution of 0.1 and generated 12 clusters for snRNA-seq by using AF dataset. Different resolutions ranging from 0.05 to 1.0 were tested manually, selecting a resolution of 0.1 for annotating cell types based on gene profiles (Fig. 1C–E). When selecting a resolution for each re-clustered population or the datasets including controls, we followed the same procedure. We re-clustered fibroblasts, endothelial cells, and cardiomyocytes (Fig. 3).

Furthermore, we compared the control and AF groups. As controls, we utilized openly published datasets of scRNA-seq or snRNA-seq obtained from healthy donors. These data were obtained from the Human Cell Atlas Data Coordination Platform with the accession number ERP123138[14]. The two datasets (AF and Control groups) were merged. Batch effects were corrected using Seurat integration with the "rpca" method. After the selection, Log-normalized with the default parameters. After removing non-immune cells, we clustered all the cells based on the integrated gene expression matrix using Seurat with a parameter resolution of 0.1 and generated 13 clusters for scRNA-seq (Fig. 1F, G and H). Then, we extracted myeloid cells from the integrated dataset and re-clustered them by the same procedure. We extracted cluster of macrophages and monocytes from the integrated dataset and re-clustered them by the same procedure (Fig. 4A).

The same procedure was performed on the combined snRNA-seq between the Control and AF groups (Supplementary Fig. 7).

In Fig. 2, we performed clustering of all cells and specifically extracted macrophages and monocytes, focusing exclusively on the AF datasets. We merged the two datasets (LA samples and PBMCs of AF) to clearly differentiate monocytes population from macrophage populations. The UMAP of PBMC was shown only in Supplementary Fig. 2E, while the UMAP of LA samples, excluding the PBMC dataset, is presented in the main figures.

RNA Velocity analyses

RNA Velocity analyses were performed by the scvelo. First, RNA Velocity utilized the raw data to count the spliced (mRNA) and un-spliced (Introns) reads for each gene, and generated a.loom file. Next, those loom files were loaded into python using scvelo.read function to generate RNA velocity data for spliced and un-spliced reads in macrophages and monocytes in LA samples of AF patients. Finally, Finally, the Seurat-prepared single-cell data was converted to the Python anndata format and merged with the velocity data, allowing the visualization of estimated velocities on UMAP plots.32

Single cell metabolism

Single-cell level metabolic analyses were performed by the sc-Metabolism package. Prior to conducting this analysis, prepare single-cell data by generating a UMAP using Seurat. Subsequently, evaluate the metabolic activity using the sc-Metabolism package on the generated data. Finally, visualize the results of the metabolic analysis on the UMAP using tools such as Dimplot to display differences in metabolic activation between clusters and Dotplot to visualize variations in metabolic activity between clusters[27,28].

Gene ontology (GO) analyses

We applied the clusterProfiler package to use gene ontology (GO) analyses for biological process based on the selected differentially expressed genes in each macrophage, fibroblasts, and endothelial cells cluster.

Cell chat analyses

Cell-cell interaction analysis was performed using the CellChat package (version 1.6.0)[34]. Signaling pathway networks were evaluated using this package.

Cell-SNP

SNP-based multiplexing, called Cell-SNP, was used for snRNA-seq. The multiplexed samples are distinguished based on their natural genetic landscapes. Genetically distinct samples can be pooled together for scRNA-seq experiments and then cells for individual samples can be separated by harnessing genetic differences. We used the reproducible Snakemake work flow[69], which was based on the best-performing combination of tools for estimating a genotype reference list of SNPs and demultiplexing samples[70].

Enzyme-linked immunosorbent assay (ELISA)

AREG and IGF-1 protein concentrations in serum samples were determined by each ELISA kit (Abcam, cat.ab222504 or R&D, cat.DG100B) according to the manufacturer's instructions. All samples were run simultaneously with identical standard curves and sensitivities.

Logistic regression analysis

Logistic regression analysis for predicting AF and persistent AF was calculated. Variables were included in the multivariable analysis if the P-values in the univariable analysis were less than 0.15, and a stepwise algorithm was used for variable selection.

Statistics and reproducibility

Wilcoxon rank-sum testing was used to compare gene expression between each cluster or sub-cluster. Kruskal−Wallis testing followed by Dunn's post hoc analysis was used to compare serum biomarkers between the control, paroxysmal AF, and persistent AF groups. Intergroup comparisons of

frequencies were analyzed by chi-squared testing. GraphPad Prism 10.1.1 and R 4.1.2 were used. All statistical analyses were two sided; $p < 0.05$ was considered statistically significant.

Reporting summary

Further information on research design is available in the Nature Portfolio Reporting Summary linked to this article.

Data availability

All sequencing data are publicly available at GSE261170. Healthy donors are obtained from Human Cell Atlas Data Coordination Platform, ERP123138[14]. R codes are available upon request from the corresponding author. The numerical source data underlying the graphs shown in the manuscript are available in Supplementary Data.

References

1. Chugh, S. S. et al. Worldwide epidemiology of atrial fibrillation: a Global Burden of Disease 2010 Study. *Circulation* **129**, 837–847 (2014).
2. Kornej, J., Börschel, C. S., Benjamin, E. J. & Schnabel, R. B. Epidemiology of atrial fibrillation in the 21st Century: novel methods and new insights. *Circ. Res.* **127**, 4–20 (2020).
3. Yamashita, T. et al. Recruitment of immune cells across atrial endocardium in human atrial fibrillation. *Circ. J.* **74**, 262–270 (2010).
4. Smorodinova, N. et al. Analysis of immune cell populations in atrial myocardium of patients with atrial fibrillation or sinus rhythm. *PLoS ONE* **12**, e0172691 (2017).
5. Suzuki, A. et al. Circulating intermediate CD14++CD16+monocytes are increased in patients with atrial fibrillation and reflect the functional remodelling of the left atrium. *Europace* **19**, 40–47 (2017).
6. Suehiro, H. et al. Circulating intermediate monocytes and atrial structural remodeling associated with atrial fibrillation recurrence after catheter ablation. *J. Cardiovasc. Electrophysiol.* **32**, 1035–1043 (2021).
7. Frangogiannis, N. G. Cardiac fibrosis. *Cardiovasc. Res.* **117**, 1450–1488 (2021).
8. Bhattacharya, M. & Ramachandran, P. Immunology of human fibrosis. *Nat. Immunol.* **24**, 1423–1433 (2023).
9. Rudolph, V. et al. Myeloperoxidase acts as a profibrotic mediator of atrial fibrillation. *Nat. Med.* **16**, 470–474 (2010).
10. Hulsmans, M. et al. Recruited macrophages elicit atrial fibrillation. *Science* **381**, 231–239 (2023).
11. Thrupp, N. et al. Single-Nucleus RNA-Seq is not suitable for detection of microglial activation genes in humans. *Cell Rep.* **32**, 108189 (2020).
12. Koenig, A. L. et al. Single-cell transcriptomics reveals cell-type-specific diversification in human heart failure. *Nat. Cardiovasc. Res.* **1**, 263–280 (2022).
13. Chaffin, M. et al. Single-nucleus profiling of human dilated and hypertrophic cardiomyopathy. *Nature* **608**, 174–180 (2022).
14. Litviňuková, M. et al. Cells of the adult human heart. *Nature* **588**, 466–472 (2020).
15. Emoto, T. et al. Single-Cell RNA sequencing reveals a distinct immune landscape of myeloid cells in coronary culprit plaques causing acute coronary syndrome. *Circulation* **145**, 1434–1436 (2022).
16. Krishnamurthy, P. et al. IL-10 inhibits inflammation and attenuates left ventricular remodeling after myocardial infarction via activation of STAT3 and suppression of HuR. *Circ. Res.* **104**, e9–e18 (2009).
17. Heymans, S. et al. Increased cardiac expression of tissue inhibitor of metalloproteinase-1 and tissue inhibitor of metalloproteinase-2 is related to cardiac fibrosis and dysfunction in the chronic pressure-overloaded human heart. *Circulation* **112**, 1136–1144 (2005).
18. Wortham, B. W. et al. Cutting Edge: CLEC5A mediates macrophage function and chronic obstructive pulmonary disease pathologies. *J. Immunol.* **196**, 3227–3231 (2016).
19. Wang, X., Hu, Y., Wang, Y., Shen, D. & Tao, G. CLEC5A knockdown protects against cardiac dysfunction after myocardial infarction by suppressing macrophage polarization, NLRP3 inflammasome activation, and pyroptosis. *Biochem. Cell Biol.* **99**, 655–665 (2021).
20. Mezache, L. et al. Vascular endothelial growth factor promotes atrial arrhythmias by inducing acute intercalated disk remodeling. *Sci. Rep.* **10**, 20463 (2020).
21. Danen, E. H. & Yamada, K. M. Fibronectin, integrins, and growth control. *J. Cell Physiol.* **189**, 1–13 (2001).
22. Klemis, V. et al. Circulating fibronectin contributes to mesangial expansion in a murine model of type 1 diabetes. *Kidney Int.* **91**, 1374–1385 (2017).
23. Ramachandran, P. et al. Resolving the fibrotic niche of human liver cirrhosis at single-cell level. *Nature* **575**, 512–518 (2019).
24. Keren-Shaul, H. et al. A unique microglia type associated with restricting development of Alzheimer's disease. *Cell* **169**, 1276–1290.e1217 (2017).
25. Patterson, M. T. et al. Trem2 promotes foamy macrophage lipid uptake and survival in atherosclerosis. *Nat. Cardiovasc. Res.* **2**, 1015–1031 (2023).
26. Jung, S. H. et al. Spatiotemporal dynamics of macrophage heterogeneity and a potential function of Trem2(hi) macrophages in infarcted hearts. *Nat. Commun.* **13**, 4580 (2022).
27. Wu, Y. et al. Spatiotemporal immune landscape of colorectal cancer liver metastasis at single-cell level. *Cancer Discov.* **12**, 134–153 (2022).
28. Xiong, J. et al. Bulk and single-cell characterisation of the immune heterogeneity of atherosclerosis identifies novel targets for immunotherapy. *BMC Biol.* **21**, 46 (2023).
29. Nicolás-Ávila, J. A. et al. A network of macrophages supports mitochondrial homeostasis in the heart. *Cell* **183**, 94–109.e123 (2020).
30. Mulder, K. et al. Cross-tissue single-cell landscape of human monocytes and macrophages in health and disease. *Immunity* **54**, 1883–1900.e1885 (2021).
31. Yerra, V. G. et al. Pressure overload induces ISG15 to facilitate adverse ventricular remodeling and promote heart failure. *J. Clin. Investig.* **133** https://doi.org/10.1172/jci161453 (2023).
32. La Manno, G. et al. RNA velocity of single cells. *Nature* **560**, 494–498 (2018).
33. Sheng, Y. et al. Deciphering mechanisms of cardiomyocytes and non-cardiomyocyte transformation in myocardial remodeling of permanent atrial fibrillation. *J. Adv. Res.* **61**, 101–117 (2023).
34. Jin, S. et al. Inference and analysis of cell-cell communication using CellChat. *Nat. Commun.* **12**, 1088 (2021).
35. Jiang, Z. et al. The role of platelet-derived growth Factor-B/Platelet-derived growth factor Receptor-β Signaling in chronic atrial fibrillation. *Cardiology* **133**, 242–256 (2016).
36. Digiacomo, G. et al. Fibronectin induces macrophage migration through a SFK-FAK/CSF-1R pathway. *Cell Adh Migr.* **11**, 327–337 (2017).
37. Chen, P. et al. Collagen VI regulates peripheral nerve regeneration by modulating macrophage recruitment and polarization. *Acta Neuropathol.* **129**, 97–113 (2015).
38. Corada, M., Morini, M. F. & Dejana, E. Signaling pathways in the specification of arteries and veins. *Arterioscler Thromb. Vasc. Biol.* **34**, 2372–2377 (2014).
39. Pruenster, M. et al. The Duffy antigen receptor for chemokines transports chemokines and supports their promigratory activity. *Nat. Immunol.* **10**, 101–108 (2009).
40. Tang, J. et al. Genetic fate mapping defines the vascular potential of endocardial cells in the adult heart. *Circ. Res.* **122**, 984–993 (2018).
41. Awwad, K. et al. Role of secreted modular calcium-binding protein 1 (SMOC1) in transforming growth factor β signalling and angiogenesis. *Cardiovasc. Res.* **106**, 284–294 (2015).

42. Yang, J. et al. Single-cell RNA sequencing reveals a mechanism underlying the susceptibility of the left atrial appendage to intracardiac thrombogenesis during atrial fibrillation. *Clin. Transl. Med.* **13**, e1297 (2023).

43. Chen, W. et al. The Notch signaling pathway regulates macrophage polarization in liver diseases. *Int. Immunopharmacol.* **99**, 107938 (2021).

44. Li, C. et al. Elevated myocardial SORBS2 and the underlying implications in left ventricular noncompaction cardiomyopathy. *EBioMedicine* **53**, 102695 (2020).

45. Zaman, R. et al. Selective loss of resident macrophage-derived insulin-like growth factor-1 abolishes adaptive cardiac growth to stress. *Immunity* **54**, 2057–2071.e2056 (2021).

46. Revelo, X. S. et al. Cardiac resident macrophages prevent fibrosis and stimulate angiogenesis. *Circ. Res.* **129**, 1086–1101 (2021).

47. Simões, F. C. et al. Macrophages directly contribute collagen to scar formation during zebrafish heart regeneration and mouse heart repair. *Nat. Commun.* **11**, 600 (2020).

48. Dick, S. A. et al. Self-renewing resident cardiac macrophages limit adverse remodeling following myocardial infarction. *Nat. Immunol.* **20**, 29–39 (2019).

49. Epelman, S. et al. Embryonic and adult-derived resident cardiac macrophages are maintained through distinct mechanisms at steady state and during inflammation. *Immunity* **40**, 91–104 (2014).

50. Sudar-Milovanovic, E. et al. Hormonal Regulation of Nitric Oxide (NO) in cardio-metabolic diseases. *Curr. Pharm. Des.* **23**, 1427–1434 (2017).

51. Macvanin, M. et al. New insights on the cardiovascular effects of IGF-1. *Front. Endocrinol.* **14**, 1142644 (2023).

52. Busch, M. et al. Relation of IGF-1 and IGFBP-3 with prevalent and incident atrial fibrillation in a population-based study. *Heart Rhythm* **16**, 1314–1319 (2019).

53. Cignarelli, A. et al. Mini review: effect of GLP-1 receptor agonists and SGLT-2 inhibitors on the Growth Hormone/IGF Axis. *Front. Endocrinol.* **13**, 846903 (2022).

54. Patel, B. et al. CCR2(+) monocyte-derived infiltrating macrophages are required for adverse cardiac remodeling during pressure overload. *JACC Basic Transl. Sci.* **3**, 230–244 (2018).

55. Monnerat, G. et al. Macrophage-dependent IL-1β production induces cardiac arrhythmias in diabetic mice. *Nat. Commun.* **7**, 13344 (2016).

56. El Khoury, N., Mathieu, S. & Fiset, C. Interleukin-1β reduces L-type Ca2+ current through protein kinase Cε activation in mouse heart. *J. Biol. Chem.* **289**, 21896–21908 (2014).

57. De Jesus, N. M. et al. Antiarrhythmic effects of interleukin 1 inhibition after myocardial infarction. *Heart Rhythm* **14**, 727–736 (2017).

58. Krisai, P. et al. Canakinumab after electrical cardioversion in patients with persistent atrial fibrillation: a pilot randomized trial. *Circ. Arrhythmia Electrophysiol.* **13**, e008197 (2020).

59. Perugorria, M. J. et al. The epidermal growth factor receptor ligand amphiregulin participates in the development of mouse liver fibrosis. *Hepatology* **48**, 1251–1261 (2008).

60. Ding, L. et al. Bone marrow CD11c+ cell-derived amphiregulin promotes pulmonary fibrosis. *J. Immunol.* **197**, 303–312 (2016).

61. Kefaloyianni, E. et al. Proximal tubule-derived amphiregulin amplifies and integrates profibrotic EGF receptor signals in kidney fibrosis. *J. Am. Soc. Nephrol.* **30**, 2370–2383 (2019).

62. Son, S. S. et al. In vivo silencing of amphiregulin by a novel effective Self-Assembled-Micelle inhibitory RNA ameliorates renal fibrosis via inhibition of EGFR signals. *Sci. Rep.* **11**, 2191 (2021).

63. Todd, J. L. et al. Amphiregulin contributes to airway remodeling in chronic allograft dysfunction after lung transplantation. *Am. J. Transpl.* **20**, 825–833 (2020).

64. Zaiss, D. M. W., Gause, W. C., Osborne, L. C. & Artis, D. Emerging functions of amphiregulin in orchestrating immunity, inflammation, and tissue repair. *Immunity* **42**, 216–226 (2015).

65. Sugita, J. et al. Cardiac macrophages prevent sudden death during heart stress. *Nat. Commun.* **12**, 1910 (2021).

66. Büttner, P. et al. Identification of central regulators of calcium signaling and ECM-Receptor interaction genetically associated with the progression and recurrence of atrial fibrillation. *Front. Genet.* **9**, 162 (2018).

67. Haissaguerre, M. et al. Spontaneous initiation of atrial fibrillation by ectopic beats originating in the pulmonary veins. *N. Engl. J. Med.* **339**, 659–666 (1998).

68. Butler, A., Hoffman, P., Smibert, P., Papalexi, E. & Satija, R. Integrating single-cell transcriptomic data across different conditions, technologies, and species. *Nat. Biotechnol.* **36**, 411–420 (2018).

69. Koster, J. & Rahmann, S. Snakemake-a scalable bioinformatics workflow engine. *Bioinformatics* **28**, 2520–2522 (2012).

70. Weber, L. M. et al. Genetic demultiplexing of pooled single-cell RNA-sequencing samples in cancer facilitates effective experimental design. *Gigascience* **10** https://doi.org/10.1093/gigascience/giab062 (2021).

Acknowledgements

Author contributions

Y.Suzuki, T.E., R.T., T.O., T.F., R.N, T.Yamashita., K.H., and K.F. conceptualized and designed the experiments. S.S. collected the atrial samples. Y.Suzuki, T.E., T. Yoshida, M.S., M.I., and M.Taniguchi, processed the samples and analyzed the single cell data. Y.Suzuki, T.E. T.Hamana, T.I., T.Hayashi, M.I., M.S., M.N., H.K., K.K, M.Takami., K.I., T.N., Y.S., H.T., K.N., K.Y., K.T., H.I., Y.N. S.Y., and A.M., collected the serum samples and analyzed the data. H.E. and E.N. captured the TEM images. Y.Suzuki and T.E. drafted the manuscript. T.E. and T.Yamashita. and K.F. revised the paper and contributed editing process. All authors approved the final manuscript.

Competing interests

The authors declare no competing interests.

Additional information

Supplementary information The online version contains supplementary material available at https://doi.org/10.1038/s42003-024-07308-w.

Correspondence and requests for materials should be addressed to Takuo Emoto.

Peer review information *Communications Biology* thanks Hui-Hua Li and the other, anonymous, reviewer(s) for their contribution to the peer review of this work. Primary Handling Editors: Kaoru Ito and Dario Ummarino. A peer review file is available.

Reprints and permissions information is available at http://www.nature.com/reprints